

Haptic-based Complementary Filter for Rigid Body Rotations

Amit Kumar¹, Domenico Campolo² and Ravi N. Banavar¹

Abstract—The non-commutative nature of 3D rotations poses well-known challenges in generalizing planar problems to three-dimensional ones, even more so in contact-rich tasks where haptic information (i.e., forces/torques) is involved. In this sense, not all learning-based algorithms that are currently available generalize to 3D orientation estimation. Non-linear filters defined on $\mathbb{SO}(3)$ are widely used with inertial measurement sensors; however, none of them have been used with haptic measurements. This paper presents a unique complementary filtering framework that interprets the geometric shape of objects in the form of superquadrics, exploits the symmetry of $\mathbb{SO}(3)$, and uses force and vision sensors as measurements to provide an estimate of orientation. The framework’s robustness and almost global stability are substantiated by a set of experiments on a dual-arm robotic setup.

I. INTRODUCTION

With the recent advancements in robotic manipulation, a big question remains: ‘If humans can perform various manipulation tasks dexterously, why can’t we program robots to do the same?’. Studies from neurobiology have proven that people with impaired tactile sensibility find it challenging to control object manipulations [1]. It is then imperative to include haptic information (sense of touch and motion) for robotic operations such as those performed by humanoids or robotic arms [2]. This haptic information aids in developing accurate controllers and observers, e.g., for manufacturing and assembly tasks [3].

Recent literature demonstrates that learning-based methods, such as neural networks, are effective for some vision-based contact-rich manipulation tasks [4]. Factors like lighting conditions, distractor objects, backgrounds, table textures, and camera positions play a role in generalizing such methods. Researchers in [5] have created a manipulation pipeline, SIMPLE, for task-aware picking, visuotactile object pose estimation, and motion planning. Given an object’s computer-aided design (CAD), it learns to pick and place an object using simulation. The visuotactile object pose estimation combines tactile images and a depth camera to update the estimate of the distribution of possible grasped object poses. Although it achieved 90% successful placements for six objects that it was tested on, authors mention a known limitation of this pipeline is that it works in open-loop. Once a visuotactile pose estimate is found, it does not update its belief of the object pose. In the traditional Finite Element

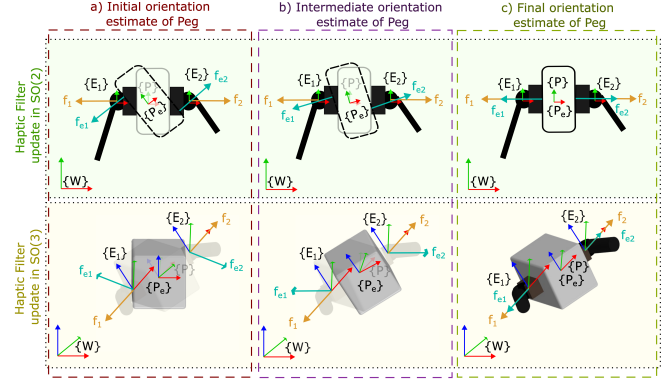


Fig. 1: Evolution of the orientation of an object, peg, based on only the haptic information from the force sensors mounted at the end-effectors ($\{E_1\}, \{E_2\}$) of the dual-robotic arm setup. The observer is defined directly on $\mathbb{SO}(3)$.

Analysis (FEA) approach, an accurate simulation may take tens of seconds [6]. Additionally, these algorithms are data-hungry and may not be practical in many time-sensitive settings. This necessitates filter designs for haptic feedback that aggregate multiple sensor readings, and reduce failures.

Several works have proposed the use of haptic filters for different robotic tasks. Cortesão *et al.* [7] have used Kalman Active Observers for robotic telemanipulation. However, contact forces are inherently non-linear [8]. Linearization of a non-linear system cannot guarantee robustness [9]. Ding *et al.* [10] present a pose estimation algorithm using tactile information from the fingertips of a gripper combined with haptic rendering models (HRMs). The CAD file of the gripper’s fingertips is used to create a voxelmap for HRM. The distance between the object and the voxel is converted into force. This gives the expected tactile responses of the object. A particle filter provides correspondences between the measured sensor information from the real geometry and the expected sensor data from the HRM. As it uses Monte Carlo simulation, this method is computationally expensive. It is well proven that human perception exploits constraints provided by the structure of the scene without reliance on quantitative, pointwise models of the image formation process [11]. It is then only natural to devise methods that interpret the geometric structure of the visual inputs for tasks such as contact-rich manipulation [12]. One such smooth geometric structure is obtained from superquadric (superellipsoid) modeling, especially useful to capture networks of (convex) rigid bodies with a relatively small number of parameters [13]. Liu *et al.* [12] have presented a robust

¹Amit Kumar and Ravi N. Banavar are with Centre for Systems and Control, Indian Institute of Technology Bombay, Mumbai, India. {amit.k.kumar, banavar}@iitb.ac.in

²Domenico Campolo is with the School of Mechanical and Aerospace Engineering, Nanyang Technological University (NTU), Singapore. d.campolo@ntu.edu.sg

method to recover superquadrics from point clouds of convex objects.

Petrovskaya *et al.* [14] proposed an efficient Bayesian approach termed Scaling Series for full 6DOF localization of an object. A touch sensor is attached to the end-effector of a robotic arm. The arm moves along the surface of the stationary object to determine its pose during the sensing phase. It then grasps the object. These methods are clearly not suitable for cases such as robotic insertion tasks where objects can move during the sensing phase.

The kinematics of an object's orientation evolves on a Lie Group [15]. Exploiting the symmetry of this underlying manifold leads to robustness. Campolo *et al.* [16] and Mahony *et al.* [9] have presented non-linear complementary filters defined directly on the matrix Lie-group representation of $\mathbb{SO}(3)$. These are widely used for estimating the orientation of an object using an Inertial Measurement Unit (IMU) attached to the body frame. The IMU provides measurements of the rate gyro, accelerometer, and magnetometer. These measurements are used to drive the estimator kinematics to the true orientation.

Larby *et al.* [17] have used Virtual Model Control to create energy-based controllers for minimally invasive surgery. These virtual springs and dampers produce controllers that are more interpretable by users. Campolo *et al.* [8], [18] used these for geometric frameworks to analyze mechanical manipulation under a quasi-static regime. Virtual springs are used to model mechanical interaction. The force generated when two objects come in contact can be estimated using Hooke's law, given a non-linear smooth spring coefficient and the inter-penetration depth. Geometric modeling techniques like superquadrics simplify the calculation of the displacement between two bodies and hence the force using Hooke's law.

In totality, developing non-linear filters defined on $\mathbb{SO}(3)$ that can aggregate multiple sensor readings, such as from the camera and force/torque sensor, in a closed loop while exploiting the geometric structure of the objects will lead to high efficiency and robustness. To our knowledge, the prior art has not addressed a haptic-based framework defined on $\mathbb{SO}(3)$. We propose a haptic-based framework that uses:

- 1) Superquadrics to model objects,
- 2) Virtual springs to estimate forces and thus provide haptic mismatch,
- 3) Vision sensor to provide orientation measurement, and
- 4) Modified non-linear complementary filter defined on $\mathbb{SO}(3)$ originally proposed in [19].

Fig. 1 shows the evolution of an object's, peg (based on peg-in-hole task), orientation based on only the haptic measurement to our observer. Section II describes the details of the problem statement along with the notations used in the paper, Section III mentions the design methodology for the haptic-based filtering framework, and Section IV presents the results obtained for different scenarios.

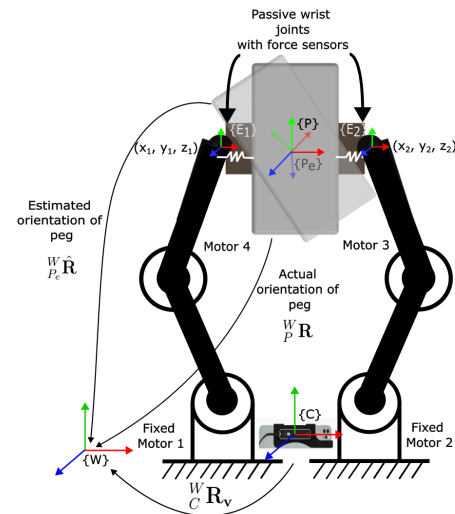


Fig. 2: Dual-robotic arm setup to test the working of designed filter on $\mathbb{SO}(3)$.

II. PROBLEM STATEMENT AND SETUP

A. Dual-Robotic Arm Setup

Consider a dual-arm setup with four motors and a peg, as shown in Fig. 2. Although we have considered a 2-link robotic arm for simplicity, our approach remains valid for any n-link manipulator. There is an extensive literature on the dual-arm setup [20]. This is mainly because it can model various tasks, such as a person picking up a box in a warehouse or a robot inserting a component into another. Our proposed filtering framework can also be used on a single robotic arm with a gripper attached; however, this limits the arm's payload capacity and, hence, its application.

Force and vision sensors are the measurements to the system. Both end-effectors have force sensors and a passive revolute joint attached to them. The geometry of the peg is fixed and is modeled as a superquadric. The vision sensor measures the orientation of the peg in 3D space. Our analysis hereon considers that the dual arms have successfully grasped the peg. This means no net force or net torque is acting on the peg.

B. Notation

The following notation is used to denote the frames of reference in the paper-

- $\{W\}$ denotes the inertial/fixed frame,
- $\{P\}$ denotes the peg's frame,
- $\{P_e\}$ denotes the estimate of peg's frame,
- $\{E_1\}$ denotes End-effector frame 1, and
- $\{E_2\}$ denotes End-effector frame 2

The following notation is used to denote the vectors in the paper-

- \mathbf{r}_0 denotes the vector from origin of $\{P_e\}$ to origin of $\{E_1\}$ in $\{P_e\}$,
- \mathbf{d}_e denotes the displacement from the surface of the peg (superquadric) to $\{E_1\}$ in $\{P_e\}$,

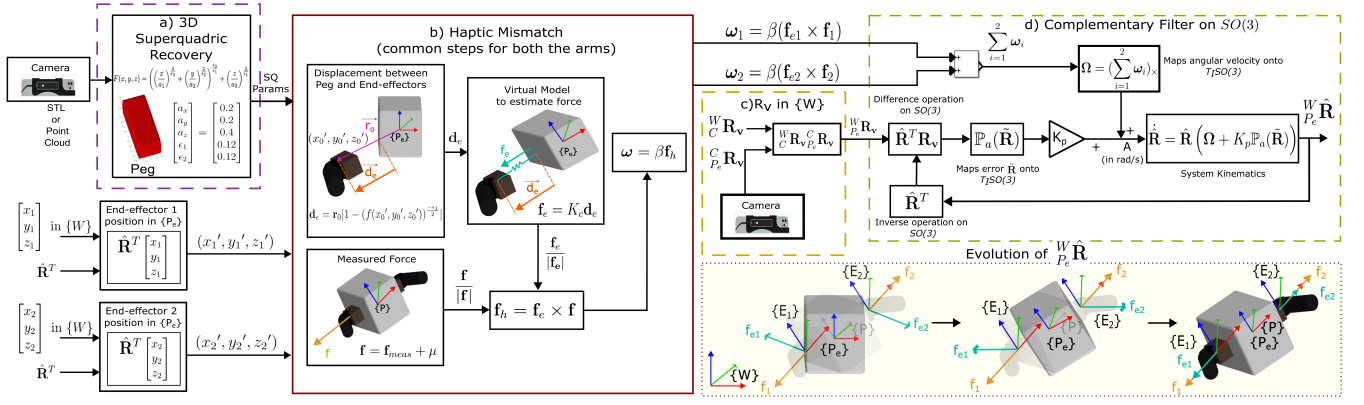


Fig. 3: Filtering framework using: a) Superquadrics to model objects, b) Virtual springs to estimate forces (haptic measurement) and calculate haptic mismatch, c) Vision sensor to provide orientation measurement, and d) Modified non-linear complementary filter defined on $\mathbb{SO}(3)$.

- f_e denotes the estimated force from the virtual spring in $\{P_e\}$,
- f denotes the actual force measurement from the force/torque sensor in $\{E_1\}$.
- f_h denotes the haptic mismatch in $\{P_e\}$, and
- ω denotes the angular velocity in $\{P_e\}$

The rotation matrix, R , and its estimate, \hat{R} for the orientation of the peg, is defined as,

$$\begin{aligned} \mathbf{R} &:= {}^W_P \mathbf{R} : \{P\} \rightarrow \{W\} \\ \hat{\mathbf{R}} &:= {}^W_{\hat{P}_e} \hat{\mathbf{R}} : \{\hat{P}_e\} \rightarrow \{W\} \end{aligned}$$

The rotation matrix, $\mathbf{R} \in \mathbb{SO}(3)$, denotes orientation of $\{P\}$ relative to $\{W\}$. Its associated lie algebra is denoted as $\mathfrak{so}(3)$. This is defined as,

$$\begin{aligned} \mathbb{SO}(3) &= \{\mathbf{R} \in SL(3, \mathbf{R}) : \mathbf{R}\mathbf{R}^T = I, \det \mathbf{R} = +1\}, \\ \mathfrak{so}(3) &= \{\mathbf{R} \in sl(3, \mathbf{R}) : \mathbf{R} + \mathbf{R}^T = 0\} \end{aligned}$$

For any two matrices $A, B \in \mathbb{R}^{n \times n}$ then the Lie-bracket (or matrix commutator) is $[A, B] = AB - BA$. Let $\omega \in \mathbb{R}^3$, then we define ω_\times as,

$$\omega_\times = \begin{pmatrix} 0 & -\omega_3 & \omega_2 \\ \omega_3 & 0 & -\omega_1 \\ -\omega_2 & \omega_1 & 0 \end{pmatrix} \in \mathfrak{so}(3)$$

For any $v \in \mathbf{R}^3$ then $\omega_\times v = \omega \times v$ is the vector cross product. \mathbb{P}_a denotes the anti-symmetric projection operator in square matrix space as,

$$\mathbb{P}_a(A) = \frac{1}{2}(A - A^T)$$

III. HAPTIC-BASED FILTERING FRAMEWORK ON $\mathbb{SO}(3)$

The filtering framework is shown in Fig. 3. Each part is discussed in the following sections.

A. Superquadric Modeling and Recovery

Superquadrics are a family of geometric primitives with a rich shape vocabulary encoded by only five parameters [12]. Superellipsoids are obtained by the spherical product of a pair of superellipses. The general expression of superquadric [13] (mainly we focus on superellipsoid) is given in equation 1.

$$f(x_0, y_0, z_0) = \left(\left(\frac{x_0}{a_x} \right)^{2/\epsilon_2} + \left(\frac{y_0}{a_y} \right)^{2/\epsilon_2} \right)^{\epsilon_2/\epsilon_1} + \left(\frac{z_0}{a_z} \right)^{2/\epsilon_1} \quad (1)$$

Authors in [12] have created a MATLAB toolbox to recover superquadrics from point clouds of convex objects. Using this toolbox, we find all the five parameters, namely- $a_x, a_y, a_z, \epsilon_1$, and ϵ_2 . This is shown in Fig. (3a)

B. Haptic Mismatch- Measurement from force sensors

As mentioned in Section II, our problem statement assumes that the dual arms have successfully grasped the peg. The force sensor gives the actual force measurement, f , and the estimated force, f_e , is calculated using virtual springs connected to the estimated orientation of the peg. There is one spring between each end-effector and the surface of the superquadric. To calculate force using Hooke's law, a radial displacement vector from the surface of the superquadric to the end-effector is required. This is calculated using equation 2 as given in [13].

$$d_e = r_o |1 - (f(x_0, y_0, z_0))^{-\frac{\epsilon_1}{2}}|, \quad d_e \in \mathbf{R}^3 \text{ and in } \{P_e\} \quad (2)$$

where, (x_0, y_0, z_0) is the position of the end-effector in $\{P_e\}$ and r_o denotes the vector from origin of $\{P_e\}$ to origin of end-effector. As the position of the end-effector is available in $\{W\}$ by using the robotic arm's defined kinematics, the position vector is pre-multiplied by $\hat{\mathbf{R}}^T$ to bring the position vector in $\{P_e\}$.

Now, the force is calculated using Hooke's law as given in equation 3.

$$\mathbf{f}_e = K_c \mathbf{d}_e \in \mathbb{R}^3 \text{ and in } \{P_e\} \quad (3)$$

where, K_c is the spring coefficient.

The force sensors attached to the end-effectors provide the force measurement, \mathbf{f}_1 , and \mathbf{f}_2 in $\{E_1\}$, and $\{E_2\}$ respectively. Since we have assumed that the peg is successfully grasped, the orientation of $\{P\}$ remains the same as $\{E_1\}$. Moreover, when $\{P_e\}$ will overlap $\{P\}$, \mathbf{f} can be considered to be in either of the frames. As no net force or torque is acting on the peg, the forces measured by both end-effectors will be anti-collinear. Both \mathbf{f} and \mathbf{f}_e are normalized. Then, the haptic mismatch [21] due to one end-effector is defined as the cross product of \mathbf{f} and \mathbf{f}_e , as given in equation 4.

$$\mathbf{f}_h = (\mathbf{f}_e \times \mathbf{f}) \in \mathbb{R}^3, |\mathbf{f}| = 1, |\mathbf{f}_e| = 1 \quad (4)$$

The goal is to drive \mathbf{f}_h to 0 which will happen when $\mathbf{f}_e = \mathbf{f}$. Now, \mathbf{f}_e will keep on changing as the peg rotates. This rotational velocity is captured through equation 5.

$$\boldsymbol{\omega} = \beta \mathbf{f}_h \in \mathbb{R}^3 \quad (5)$$

where, β is the admittance coefficient. These steps are shown in Fig. (3b).

C. Measurement from vision sensor

The vision sensor measures the orientation of the peg in its own frame, $\{C\}$. This orientation is defined as,

$$\mathbf{R}_v := {}^C_{P_e} \mathbf{R}_v : \{P_e\} \rightarrow \{C\}$$

As $\{C\}$ is static with respect to $\{W\}$, we obtain the orientation of the peg in the world frame using equation 6. This is shown in Fig. (3c).

$${}^W_{P_e} \mathbf{R}_v = ({}^W_C \mathbf{R}_v) ({}^C_{P_e} \mathbf{R}_v) \in \mathbb{SO}(3) \quad (6)$$

D. Complementary filter on $\mathbb{SO}(3)$

We take inspiration from the passive complementary filter defined in [9] and modify it to suit our problem. The block diagram of the filter is shown in Fig. (3d). The rotation kinematics of the true system are given in equation 7.

$$\dot{\mathbf{R}} = \mathbf{R}\boldsymbol{\Omega}, \mathbf{R}(0) = \mathbf{R}_0 \quad (7)$$

where, $\boldsymbol{\Omega} = \boldsymbol{\omega}_\times$. The kinematics of our filter is given in equation 8.

$$\dot{\hat{\mathbf{R}}} = \hat{\mathbf{R}} \left(\boldsymbol{\Omega} + K_p \mathbb{P}_a(\tilde{\mathbf{R}}) \right), \hat{\mathbf{R}}(0) = \hat{\mathbf{R}}_0 \quad (8)$$

where $K_p > 0$ is a positive gain. The observer kinematics include a prediction term, $\boldsymbol{\Omega}$, based on the force sensors measurement and an innovation term, $K_p \mathbb{P}_a(\tilde{\mathbf{R}})$ based on the error $\tilde{\mathbf{R}}$, defined using vision sensor measurement.

We start by defining the error on $\mathbb{SO}(3)$. The goal of our observer is to drive $\tilde{\mathbf{R}} \rightarrow \mathbf{R}$. The error is given in equation 9.

$$\tilde{\mathbf{R}} = \hat{\mathbf{R}}^T \mathbf{R}_v \in \mathbb{SO}(3) \quad (9)$$

The error $\tilde{\mathbf{R}}$ is mapped to the tangent space of $\mathbb{SO}(3)$, i.e., $\mathfrak{so}(3)$ in the filter design. This is done using the anti-symmetric projection operator, \mathbb{P}_a , defined in Section II. Note that the $\mathbb{P}_a(\tilde{\mathbf{R}})$ is invariant under the adjoint map [19] as given in equation 10.

$$\text{Ad}_{\tilde{\mathbf{R}}} \mathbb{P}_a(\tilde{\mathbf{R}}) = \tilde{\mathbf{R}} \mathbb{P}_a(\tilde{\mathbf{R}}) \tilde{\mathbf{R}}^T = \mathbb{P}_a(\tilde{\mathbf{R}}) \quad (10)$$

We can hence consider, $\mathbb{P}_a(\tilde{\mathbf{R}})$ in $\{P_e\}$ as given in equation 11.

$$\mathbb{P}_a(\tilde{\mathbf{R}}) = \frac{1}{2}(\tilde{\mathbf{R}} - \tilde{\mathbf{R}}^T) \in \mathfrak{so}(3) \text{ and in } \{P_e\} \quad (11)$$

Since we have two end effectors, we get two values of $\boldsymbol{\omega}$, as defined in equation 5, for our dual-arm system. These are added together and used for the prediction part. As $\boldsymbol{\omega} \in \mathbb{R}^3$, it is mapped to $\mathfrak{so}(3)$ using the $(\)_\times$ operator as defined in Section II. Hence,

$$\boldsymbol{\Omega} = \left(\sum_{i=1}^2 \boldsymbol{\omega}_i \right)_\times \in \mathfrak{so}(3) \quad (12)$$

The admittance coefficients, β , for each arm and proportional gain, K_p , are the weights of the complementary filter. These weights can be adjusted based on the trust in the measurements from the force and vision sensors. The following non-linear stability theorem is taken verbatim from [9].

Theorem 3.1: Consider the kinematics of rotation as defined in equation 7 for $\mathbf{R}(t) \in \mathbb{SO}(3)$ and measurements given by equations (5) and (6). $\boldsymbol{\Omega} \in \mathfrak{so}(3)$ is defined using equation 12. Let $\hat{\mathbf{R}}(t)$ denote the solution of equation 8. Define error, $\tilde{\mathbf{R}}$, as given in equation 9. Assume that $\boldsymbol{\omega}$ is bounded, absolutely continuous and that the pair of signals $(\boldsymbol{\omega}(t), \tilde{\mathbf{R}})$ are asymptotically independent. Define the set, $\mathbb{U}_0 \subseteq \mathbb{SO}(3)$ of all initial conditions for which the kinematic equation 8 is unstable. This is given by,

$$\mathbb{U}_0 = \{ \tilde{\mathbf{R}} \mid \text{tr}(\tilde{\mathbf{R}}) = -1 \} \quad (13)$$

Then, the error, $\tilde{\mathbf{R}}(t)$ is locally exponentially stable to \mathbf{I} and for $\tilde{\mathbf{R}}_0 \notin \mathbb{U}_0$, $\tilde{\mathbf{R}}(t)$ converges to $\mathbf{R}(t)$.

IV. RESULTS

Using MATLAB's Simulink environment, we have tested the filtering framework shown in Figure 3. The simulations were performed with a fixed time step of 0.1s and automatic solver selection. Results are shown in Fig. 4. Variables with subscripts 1 and 2 denote each of the end-effectors, respectively. $K_{c1} = 1$, $K_{c2} = 1$, $\beta_1 = -1$, $\beta_2 = -1$, $\mathbf{f}_1 =$

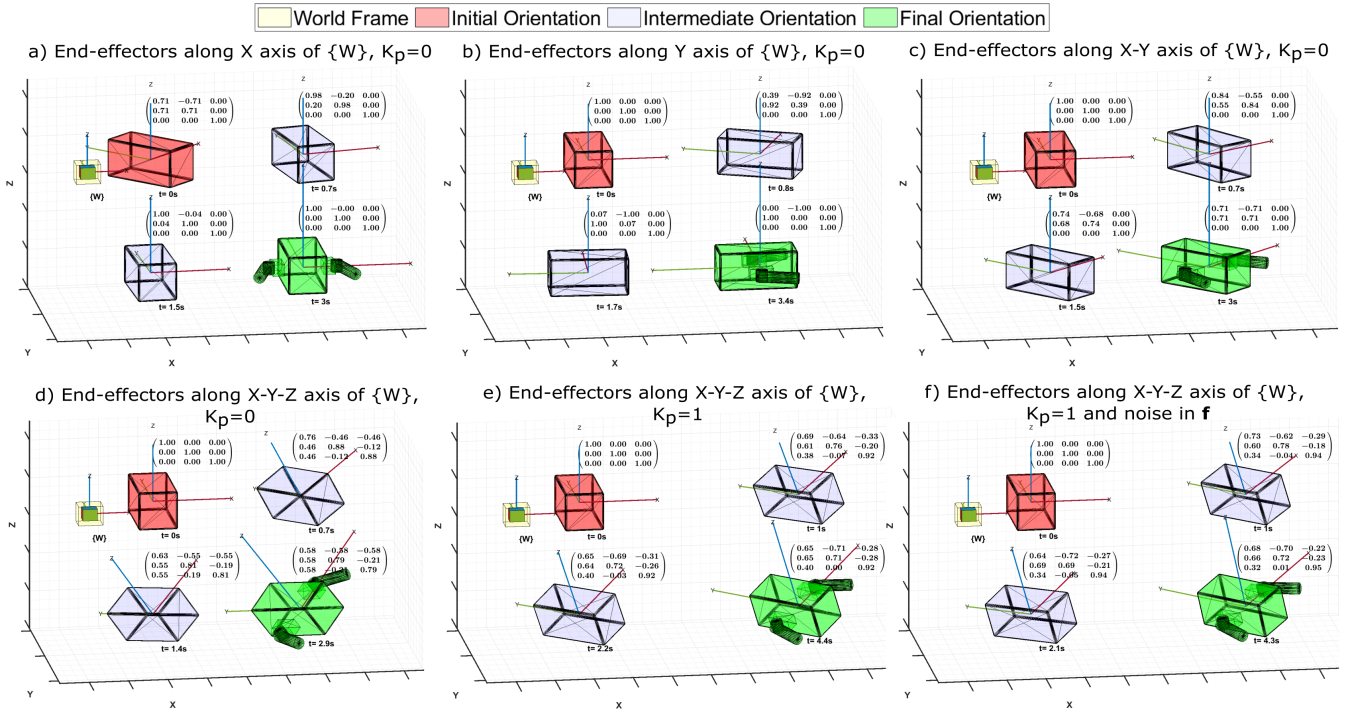


Fig. 4: Evolution of $\hat{\mathbf{R}}$ for different cases based on our designed filtering framework on $\mathbb{S}\mathbb{O}(3)$.

$\begin{bmatrix} -1 \\ 0 \\ 0 \end{bmatrix}$, and $\mathbf{f}_2 = \begin{bmatrix} 1 \\ 0 \\ 0 \end{bmatrix}$ for all the cases. We have followed the Z-Y-X rotation order and assumed anti-clockwise rotation about each axis to be positive.

A. 2D: End-effectors along X axis of $\{W\}$, $K_p = 0$

Consider the case when the end-effectors have grasped the peg along the X-axis of $\{W\}$ and the weight of the measurement from the vision sensor (K_p) is set to 0. Hence,

$$\begin{bmatrix} x_1 \\ y_1 \\ z_1 \end{bmatrix} = \begin{bmatrix} -0.3 \\ 0 \\ 0 \end{bmatrix}, \quad \begin{bmatrix} x_2 \\ y_2 \\ z_2 \end{bmatrix} = \begin{bmatrix} 0.3 \\ 0 \\ 0 \end{bmatrix}, \quad \hat{\mathbf{R}}_0 = \begin{bmatrix} 0.71 & -0.71 & 0 \\ 0.71 & 0.71 & 0 \\ 0 & 0 & 1 \end{bmatrix}$$

We can observe in Fig. (4a) that $\hat{\mathbf{R}}$ settles close to I satisfying the measurements from the force sensors.

B. 2D: End-effectors along Y axis of $\{W\}$, $K_p = 0$

In this case, the end-effectors have grasped the peg along the Y-axis of $\{W\}$ and $K_p = 0$. Hence,

$$\begin{bmatrix} x_1 \\ y_1 \\ z_1 \end{bmatrix} = \begin{bmatrix} 0 \\ -0.3 \\ 0 \end{bmatrix}, \quad \begin{bmatrix} x_2 \\ y_2 \\ z_2 \end{bmatrix} = \begin{bmatrix} 0 \\ 0.3 \\ 0 \end{bmatrix}, \quad \hat{\mathbf{R}}_0 = \begin{bmatrix} 1 & 0 & 0 \\ 0 & 1 & 0 \\ 0 & 0 & 1 \end{bmatrix}$$

We can observe in Fig. (4b) that $\hat{\mathbf{R}}$ settles to $\begin{bmatrix} 0 & -1 & 0 \\ 1 & 0 & 0 \\ 0 & 0 & 1 \end{bmatrix}$ satisfying the measurements from the force sensors.

C. 2D: End-effectors along X-Y axis of $\{W\}$, $K_p = 0$

In this case, the end-effectors have grasped the peg along the X-Y axis of $\{W\}$ and $K_p = 0$. Hence,

$$\begin{bmatrix} x_1 \\ y_1 \\ z_1 \end{bmatrix} = \begin{bmatrix} -0.3 \\ -0.3 \\ 0 \end{bmatrix}, \quad \begin{bmatrix} x_2 \\ y_2 \\ z_2 \end{bmatrix} = \begin{bmatrix} 0.3 \\ 0.3 \\ 0 \end{bmatrix}, \quad \hat{\mathbf{R}}_0 = \begin{bmatrix} 1 & 0 & 0 \\ 0 & 1 & 0 \\ 0 & 0 & 1 \end{bmatrix}$$

We can observe in Fig. (4c) that $\hat{\mathbf{R}}$ settles to $\begin{bmatrix} 0.71 & -0.71 & 0 \\ 0.71 & 0.71 & 0 \\ 0 & 0 & 1 \end{bmatrix}$ satisfying the measurements from the force sensors.

D. 3D: End-effectors along X-Y-Z axis of $\{W\}$, $K_p = 0$

In this case, the end-effectors have grasped the peg along the X-Y-Z axis of $\{W\}$ and $K_p = 0$. Hence,

$$\begin{bmatrix} x_1 \\ y_1 \\ z_1 \end{bmatrix} = \begin{bmatrix} -0.3 \\ -0.3 \\ -0.3 \end{bmatrix}, \quad \begin{bmatrix} x_2 \\ y_2 \\ z_2 \end{bmatrix} = \begin{bmatrix} 0.3 \\ 0.3 \\ 0.3 \end{bmatrix}, \quad \hat{\mathbf{R}}_0 = \begin{bmatrix} 1 & 0 & 0 \\ 0 & 1 & 0 \\ 0 & 0 & 1 \end{bmatrix}$$

To reach the end-effector positions described above, the peg is rotated by 45° along the Z axis and then -45° along the Y axis. Euler angle representation, yaw(ψ), pitch(θ), and roll(ϕ) is also mentioned for easier understanding. Using Fig. (4d) we get,

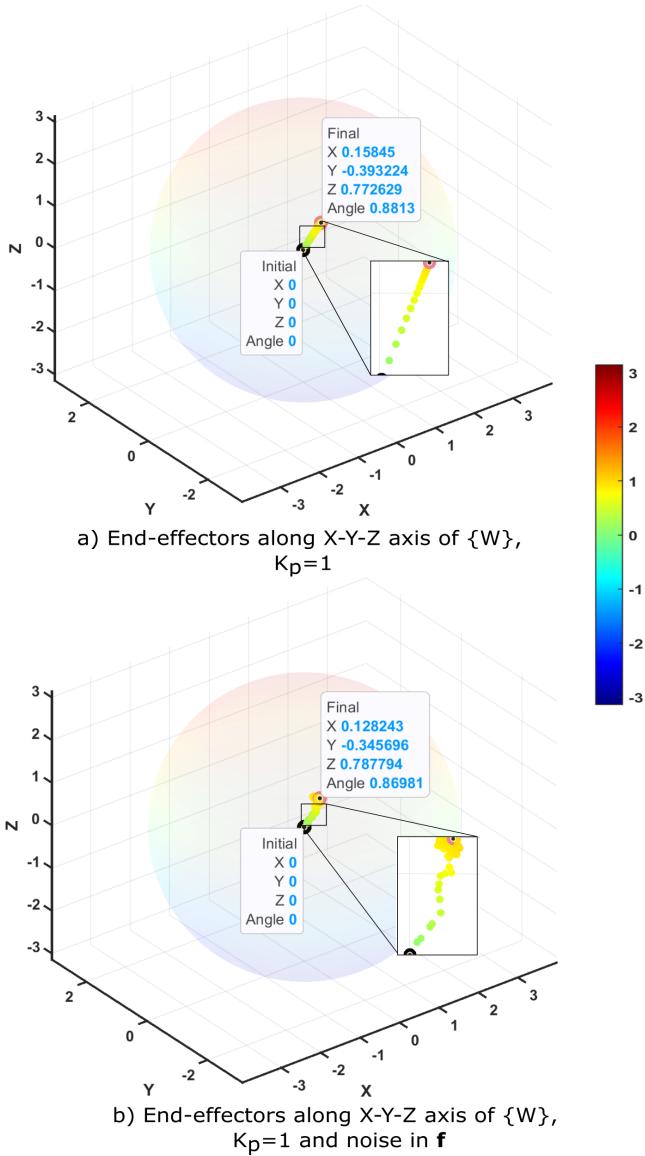


Fig. 5: π -ball axis-angle representation of $\hat{\mathbf{R}}$ a) Without noise in \mathbf{f} , and b) With noise in \mathbf{f} .

$$\mathbf{R} = \begin{bmatrix} 0.50 & -0.71 & -0.50 \\ 0.50 & 0.71 & -0.50 \\ 0.71 & 0 & 0.71 \end{bmatrix} \text{ or } \begin{bmatrix} \psi \\ \theta \\ \phi \end{bmatrix} = \begin{bmatrix} 0.78 \\ -0.78 \\ 0 \end{bmatrix},$$

$$\hat{\mathbf{R}} = \begin{bmatrix} 0.58 & -0.58 & -0.58 \\ 0.58 & 0.79 & -0.21 \\ 0.58 & -0.21 & 0.79 \end{bmatrix} \text{ or } \begin{bmatrix} \psi \\ \theta \\ \phi \end{bmatrix} = \begin{bmatrix} 0.78 \\ -0.61 \\ 0.26 \end{bmatrix}$$

The error between the observed and true rotation matrix is simply $\hat{\mathbf{R}}^T \mathbf{R}$. Converting to Euler angles, we get $(0, -0.17, 0.26)$. This is due to the integration solver settings in MATLAB and the initial condition set.

E. 3D: End-effectors along X-Y-Z axis of $\{W\}$, $K_p = 1$

In addition to the initial conditions for Case D, the weight of the measurement from the vision sensor (K_p) is

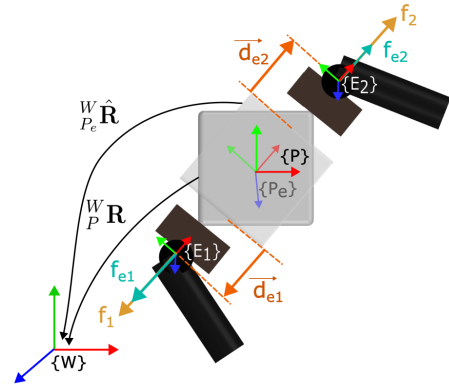


Fig. 6: Representation of a scenario where the end-effectors grasp the peg along the corners.

considered to be 1. Suppose,

$$\mathbf{R}_v = \begin{bmatrix} 0.71 & -0.71 & 0 \\ 0.71 & 0.71 & 0 \\ 0 & 0 & 1 \end{bmatrix}, \begin{bmatrix} \psi \\ \theta \\ \phi \end{bmatrix} = \begin{bmatrix} 0.78 \\ 0 \\ 0 \end{bmatrix}$$

From Fig. (4e) we get,

$$\hat{\mathbf{R}} = \begin{bmatrix} 0.65 & -0.71 & -0.28 \\ 0.65 & 0.71 & -0.28 \\ 0.40 & 0 & 0.92 \end{bmatrix}, \begin{bmatrix} \psi \\ \theta \\ \phi \end{bmatrix} = \begin{bmatrix} 0.78 \\ -0.41 \\ 0 \end{bmatrix}$$

The θ angle of $\hat{\mathbf{R}}$ in Case D is -0.61 (say θ_1) while that of Case E is -0.41 (say θ_2). This is due to the weighting factors, $|\beta|$ and K_p , which are both set to 1. We clearly see,

$$\theta_2 = \frac{|\beta_1| + |\beta_2|}{|\beta_1| + |\beta_2| + K_p} \theta_1 \quad (14)$$

Equation 14 showcases the complementary functionality of our designed filter.

F. 3D: End-effectors along X-Y-Z axis of $\{W\}$, $K_p = 1$ and noise in \mathbf{f}

Gaussian noise, with parameters ($\mu = 0, \sigma^2 = 0.5$, sample time = 1) and different seeds for each component, is added to the measured force, \mathbf{f} , to analyze the performance of the filter under noisy measurements. Evolution of $\hat{\mathbf{R}}$ is shown in Fig. (4f). For clarity, this is also shown in the π -ball axis-angle representation of $\hat{\mathbf{R}}$ in Fig. 5. The weights can be adjusted for better performance based on the noise characteristics of the sensors.

G. 3D: End-effectors grasp the peg along the corners of the peg

Consider a possible scenario where the end-effectors grasp the peg at the corners. If $\hat{\mathbf{R}}_0$ is set as shown in Fig. 6, the haptic mismatch, \mathbf{f}_n , may turn out to be $\mathbf{0}$ even when $\hat{\mathbf{R}} \neq \mathbf{R}$. To get \mathbf{f}_1 in $\{P\}$, the rotation, ${}^P_{E1} \mathbf{R}$ is required. An estimate of this can be found using the vision sensor. ${}^P_{E1} \hat{\mathbf{R}} \mathbf{f}_1$ will give the rough measurement in $\{P\}$. The rest of the filtering framework remains as is.

V. CONCLUSION AND FUTURE WORK

This paper presents a filtering framework defined on $\mathbb{SO}(3)$ that incorporates measurements from force and vision sensors to estimate the orientation of a grasped object. Much like human perception, the geometric structure of the object is encoded in the framework using superquadrics. It is validated on a simulated dual-robotic arm setup. Various cases have been detailed that highlight the convergence and robustness of the filter along with its complementary action. Future work will focus on 6-DOF pose estimation defined on $\mathbb{SE}(3)$, incorporating friction in the analysis and testing on hardware.

VI. ACKNOWLEDGMENTS

The authors would sincerely like to thank Indian Institute of Technology Bombay, Mumbai, and Nanyang Technological University (NTU), Singapore, for providing the necessary resources to carry out this research.

REFERENCES

- [1] R. Johansson and J. Flanagan, "Coding and use of tactile signals from the fingertips in object manipulation tasks," *Nature reviews. Neuroscience*, vol. 10, pp. 345–59, 05 2009.
- [2] S. H. Turlapati and D. Campolo, "Towards haptic-based dual-arm manipulation," *Sensors*, vol. 23, no. 1, 2023. [Online]. Available: <https://www.mdpi.com/1424-8220/23/1/376>
- [3] L. Yang, M. Z. Ariffin, B. Lou, C. Lv, and D. Campolo, "A planning framework for robotic insertion tasks via hydroelastic contact model," *Machines*, vol. 11, no. 7, 2023. [Online]. Available: <https://www.mdpi.com/2075-1702/11/7/741>
- [4] A. Xie, L. Lee, T. Xiao, and C. Finn, "Decomposing the generalization gap in imitation learning for visual robotic manipulation," in *2024 IEEE International Conference on Robotics and Automation (ICRA)*, 2024, pp. 3153–3160.
- [5] M. Bauza, A. Bronars, Y. Hou, I. Taylor, N. Chavan-Dafle, and A. Rodriguez, "Simple, a visuotactile method learned in simulation to precisely pick, localize, regrasp, and place objects," *Science Robotics*, vol. 9, no. 91, p. eadi8808, 2024. [Online]. Available: <https://www.science.org/doi/abs/10.1126/scirobotics.adf8808>
- [6] Y. Narang, K. Storey, I. Akinola, M. Macklin, P. Reist, L. Wawrzyniak, Y. Guo, A. Moravanszky, G. State, M. Lu, A. Handa, and D. Fox, "Factory: Fast Contact for Robotic Assembly," in *Proceedings of Robotics: Science and Systems*, New York City, NY, USA, June 2022.
- [7] R. Cortesao, J. Park, and O. Khatib, "Real-time adaptive control for haptic telemanipulation with kalman active observers," *IEEE Transactions on Robotics*, vol. 22, no. 5, pp. 987–999, 2006.
- [8] D. Campolo and F. Cardin, "A geometric framework for quasi-static manipulation of a network of elastically connected rigid bodies," *Applied Mathematical Modelling*, vol. 143, p. 116003, 2025. [Online]. Available: <https://www.sciencedirect.com/science/article/pii/S0307904X25000782>
- [9] R. Mahony, T. Hamel, and J.-M. Pfimlin, "Nonlinear complementary filters on the special orthogonal group," *IEEE Transactions on Automatic Control*, vol. 53, no. 5, pp. 1203–1218, 2008.
- [10] Y. Ding, J. Bonse, R. Andre, and U. Thomas, "In-hand grasping pose estimation using particle filters in combination with haptic rendering models," *International Journal of Humanoid Robotics*, vol. 15, no. 01, p. 1850002, 2018. [Online]. Available: <https://doi.org/10.1142/S0219843618500020>
- [11] A. P. Pentland, "Perceptual organization and the representation of natural form," *Artificial Intelligence*, vol. 28, no. 3, pp. 293–331, 1986. [Online]. Available: <https://www.sciencedirect.com/science/article/pii/0004370286900524>
- [12] W. Liu, Y. Wu, S. Ruan, and G. S. Chirikjian, "Robust and accurate superquadric recovery: a probabilistic approach," in *2022 IEEE/CVF Conference on Computer Vision and Pattern Recognition (CVPR)*, 2022, pp. 2666–2675.
- [13] A. Jaklic, A. Leonardis, and F. Solina, *Segmentation and Recovery of Superquadrics*. Springer, 2000.
- [14] A. Petrovskaya and O. Khatib, "Global localization of objects via touch," *IEEE Transactions on Robotics*, vol. 27, no. 3, pp. 569–585, 2011.
- [15] A. A. Joshi, D. H. S. Maithripala, and R. N. Banavar, "A bundle framework for observer design on smooth manifolds with symmetry," *Journal of Geometric Mechanics*, vol. 13, no. 2, pp. 247–271, 2021. [Online]. Available: <https://www.aims sciences.org/article/id/f089b456-a4e9-4204-871a-0109cc7aaae8>
- [16] D. Campolo, F. Keller, and E. Guglielmelli, "Inertial/magnetic sensors based orientation tracking on the group of rigid body rotations with application to wearable devices," in *2006 IEEE/RSJ International Conference on Intelligent Robots and Systems*, 2006, pp. 4762–4767.
- [17] D. Larby and F. Forni, "A generalized approach to impedance control design for robotic minimally invasive surgery," *IFAC-PapersOnLine*, vol. 56, no. 2, pp. 8548–8555, 2023, 22nd IFAC World Congress. [Online]. Available: <https://www.sciencedirect.com/science/article/pii/S2405896323003531>
- [18] D. Campolo and F. Cardin, "Quasi-static mechanical manipulation as an optimal process," in *2023 62nd IEEE Conference on Decision and Control (CDC)*, 2023, pp. 4753–4758.
- [19] R. Mahony, T. Hamel, and J.-M. Pfimlin, "Complementary filter design on the special orthogonal group $so(3)$," in *Proceedings of the 44th IEEE Conference on Decision and Control*, 2005, pp. 1477–1484.
- [20] E. Merlo, M. Lagomarsino, and A. Ajoudani, "Information-theoretic detection of bimanual interactions for dual-arm robot plan generation," *IEEE Robotics and Automation Letters*, pp. 1–8, 2025.
- [21] S. H. Turlapati, D. Accoto, and D. Campolo, "Haptic manipulation of 3d scans for geometric feature enhancement," *Sensors*, vol. 21, no. 8, 2021. [Online]. Available: <https://www.mdpi.com/1424-8220/21/8/2716>